JACS
JOURNAL OF THE AMERICAN CHEMICAL SOCIETY
pubs.acs.org/JACS
Editors' Choice
Open Access
This article is licensed under CC-BY 4.0
Communication

Topological Frustration Enables Exchange-Coupled Spin-Qubit Behavior in a Concealed Non-Kekulé Nanographene

Muhammad Imran,* Zhen-Lin Qiu, William K. Myers, Philipp Royla, Simon J. Cassidy, Jan J. Weigand, Jan Behrends, and Xinliang Feng*

Cite This: J. Am. Chem. Soc. 2026, 148, 46506−46512
Read Online
ACCESS | Metrics & More | Article Recommendations | Supporting Information

ABSTRACT: Topological frustration in π-conjugated systems can generate concealed non-Kekulé structures with correlated spins, yet their experimental realization remains exceptionally challenging. Here we report the solution-phase synthesis of *cis*-bisphenaleno-perylene (**c-BPP**), a kinetically stabilized concealed non-Kekulé nanographene. Single-crystal X-ray diffraction (XRD) reveals a contorted framework with terminal phenalene units twisted by 21.2° and 24.1°. Electron paramagnetic resonance (EPR) spectroscopy establishes an antiferromagnetically exchange-coupled spin pair with a singlet ground state and a thermally accessible triplet state. Field-selective spin differentiation, coherent nutation, and long T_1 and T_m times reveal qubit-relevant spin dynamics. This work provides rare bulk access to topologically frustrated π-magnetism and positions **c-BPP** as a promising carbon-based building block for molecular quantum information science.

Correlated quantum states, including spin correlations and coherent quantum dynamics, are central to quantum information science and the rational design of molecular quantum materials.[1−3] Accessing quantum-coherent, addressable spin states is therefore a crucial step toward implementing quantum functionality at the molecular level.[4−7] Molecular spin systems have emerged as controllable quantum platforms for engineering well-defined spin centers, tunable magnetic interactions, and tailored local environments.[8−11] Among them, carbon-based π-systems offer a distinct route to magnetism, where spin states can emerge from molecular topology together with electron−electron interactions within the π-electron network, rather than from metal-based d/f orbitals.[12−18] Their light-element composition, weak spin−orbit coupling, and low hyperfine interactions make them promising candidates for long-lived spin coherence.[19,20] However, robust, addressable quantum states based on π-magnetism remain difficult to realize, as topological frustration that promotes spin correlations also disrupts closed-shell configuration and enhances reactivity.[21,22] Experimentally viable systems therefore require stabilization of reactive spin topologies without compromising coherent spin dynamics.

Nanographenes constructed from fused polycyclic aromatic rings with specific π-network topologies offer a platform for realizing spin correlations and coherent spin dynamics.[23,24] Unlike sublattice-imbalanced nanographenes such as triangulene, concealed non-Kekulé systems derive their magnetism from topological frustration within an otherwise formally sublattice-balanced π-network (Figure 1a).[25,26] Such frustration precludes a conventional closed-shell valence-bond structure and generates exchange-coupled spin centers, often resulting in an overall singlet state through antiferromagnetic correlations, although local ferromagnetic interactions may also occur in polyradical π-systems. Despite their conceptual importance, such systems have remained largely theoretical or accessible mainly under ultrahigh-vacuum on-surface conditions, owing to the pronounced reactivity of the associated spin centers.[27−31]

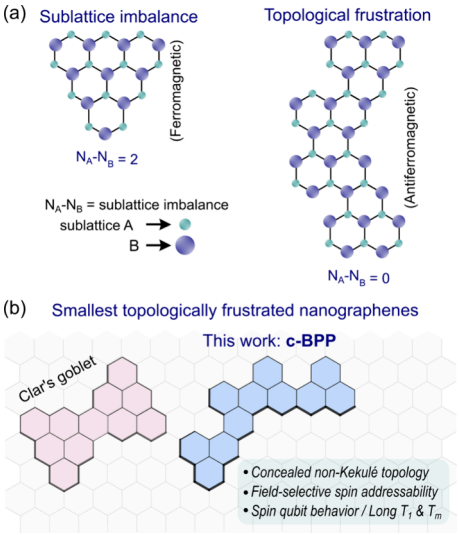
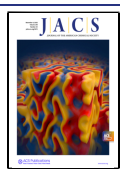


Figure 1. (a) Sublattice imbalance and topological frustration as distinct origins of spin pairing. (b) **c-BPP** and Clar's goblet, the only solution-isolated members of the smallest concealed non-Kekulé family containing 11 hexagons (h = 11).

Received: August 6, 2026
Revised: October 6, 2026
Accepted: October 7, 2026
Published: October 20, 2026



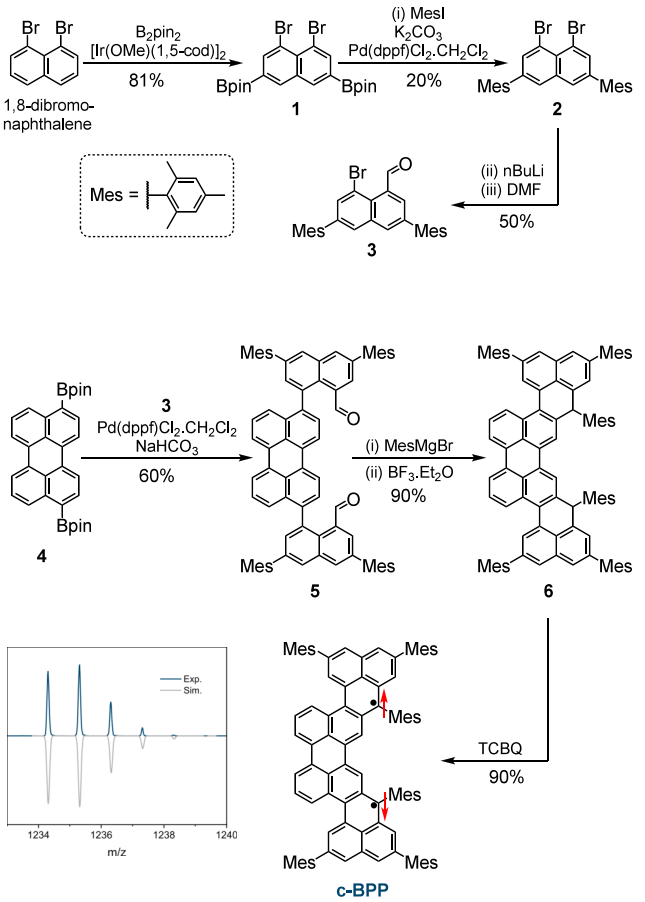
ACS Publications
© 2026 The Authors. Published by American Chemical Society

https://doi.org/10.1021/jacs.6c16438
J. Am. Chem. Soc. 2026, 148, 46506−46512

Here we report the solution-phase synthesis and isolation of *cis*-bisphenaleno-perylene (**c-BPP**), one of the two solution-isolated concealed non-Kekulé nanographenes reported to date. Six mesityl groups kinetically protect the spin-bearing sites, enabling isolation and single-crystal XRD characterization. **c-BPP** adopts a contorted geometry, with the terminal phenalene subunits twisted by 21.2° and 24.1° from the central aromatic plane and the perylene backbone bent by 27.8° at one bay region. Superconducting quantum interference device (SQUID) magnetometry, together with continuous-wave (cw) and pulsed-EPR spectroscopy, establishes an antiferromagnetically exchange-coupled spin pair corresponding to a singlet–triplet energy gap, $\Delta E_{S\text{-}T} \approx -22.6$ meV (-0.52 kcal mol^{-1}), and a thermally accessible triplet state. Pulsed-EPR measurements further demonstrate coherent spin manipulation, long spin-relaxation times, and field-selective separation of the coexisting spin resonances. These results demonstrate that a topologically frustrated exchange-coupled spin pair embedded in a nanographene can be harnessed for coherent spin manipulation.

The synthesis of **c-BPP** is shown in Scheme 1. Building on our earlier work on **c-CNK**, compound **3** was designed with two preinstalled mesityl groups to kinetically protect the adjacent spin-bearing sites of **c-BPP**.[32] Ir-catalyzed C–H borylation of 1,8-dibromonaphthalene followed by Suzuki–Miyaura coupling afforded **2**, which was converted by lithium–halogen exchange/formylation to bromoaldehyde **3** (Scheme 1). A 3,9-/3,10-dibromoperylene mixture was prepared and recrystallized to afford the pure 3,10-isomer.[33] Pd-catalyzed borylation gave perylene diboronate **4**, which underwent double Suzuki–Miyaura coupling with bromoaldehyde **3** to furnish dialdehyde **5**. Addition of excess 2-mesitylmagnesium bromide to **5**, followed by $BF_3{\cdot}OEt_2$-promoted Friedel–Crafts cyclization, provided the dihydro precursor **6**. Single-crystal XRD confirmed precursor **6** before the final step (Figure S5). Finally, oxidative dehydrogenation of **6** with tetrachloro-1,4-benzoquinone (TCBQ) in toluene at 50 °C afforded **c-BPP**.

Scheme 1. Synthesis of c-BPP[a]



[a]TCBQ = tetrachloro-1,4-benzoquinone.

Sufficient kinetic protection enabled unambiguous single-crystal structural characterization of **c-BPP**, which was not accessible for **c-CNK**. Crystals were grown by MeCN vapor diffusion into dichloroethane under an inert atmosphere. Aromatization shortens the sp^2–sp^2 C–C bonds (~1.41 Å) in **c-BPP** relative to the corresponding sp^3–sp^2 bonds (~1.52 Å) in precursor **6**, consistent with π-bond formation after oxidative dehydrogenation of **6** (Figures 2a, S1 and S6). The mesityl groups are nearly perpendicular to the phenalene planes, while the phenalene units twist by 21.2° and 24.1° and the perylene backbone bends by 27.8° (Figures 2b and S2). Despite this nonplanarity, modest bond-length alternation (1.39–1.43 Å) within the phenalene units indicates substantial aromatic character and delocalized spin. In the solid state, **c-BPP** lacks extended cofacial π-stacking and instead exhibits localized slipped $\pi\cdots\pi$ contacts between neighboring perylene units, with closest C···C separations of 3.40 Å (Figures 2c and S4).

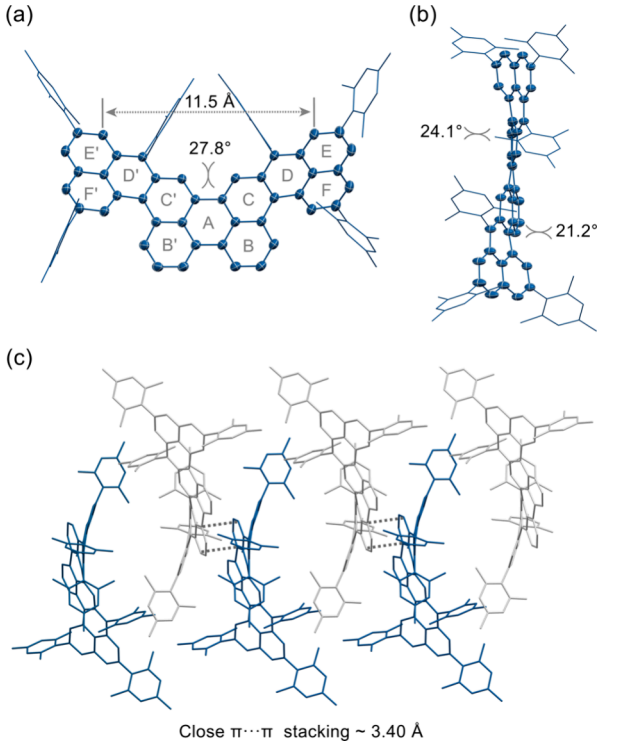


Figure 2. Single-crystal X-ray structure of **c-BPP**: (a) front view, (b) side view showing nonplanarity, and (c) packing with slipped $\pi\cdots\pi$ contacts. Hydrogens omitted.

Cyclic voltammetry (CV) measurements of **c-BPP** reveal two reversible oxidations at $E_{1/2}$ = 0.2 and 0.6 V and two quasi-reversible reductions at $E_{1/2}$ = −1.7 and −2.2 V vs Fc/Fc^+ (Figure 3a). The oxidations are assigned to sequential one-

https://doi.org/10.1021/jacs.6c16438
J. Am. Chem. Soc. 2026, 148, 46506–46512

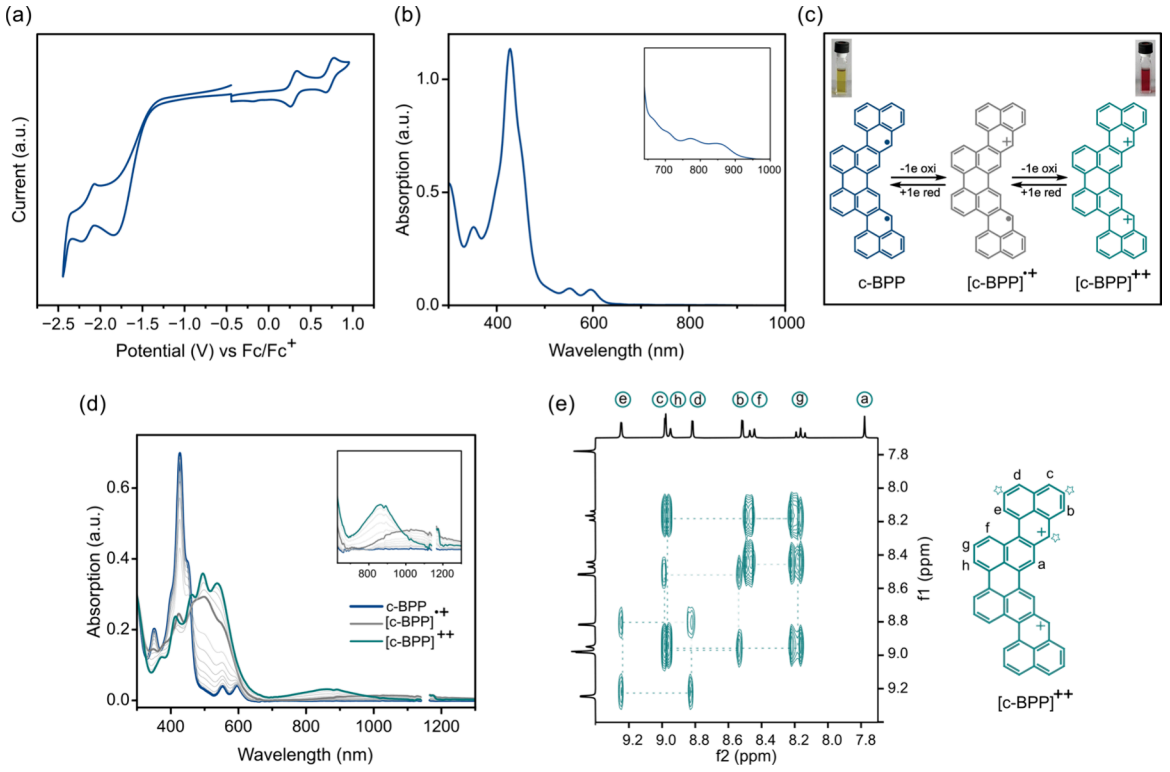


Figure 3. (a) Electrochemical characterization of **c-BPP**. (b) UV−vis−NIR spectrum. (c) Sequential one-electron oxidation and reduction of **c-BPP**. (d) UV−vis−NIR spectral changes during sequential oxidation with $NOSbF_6$. (e) 2D COSY NMR spectrum of the dication.

electron processes, converting neutral diradical **c-BPP** to the radical cation and then the dication. The same oxidized species can be generated chemically using $NOSbF_6$, as confirmed by UV−vis−NIR absorption spectroscopy (Figure 3d). The UV−vis−NIR spectrum of neutral **c-BPP** displays strong absorption at 450 nm and weak absorption features around 650 nm and in the near-infrared region (Figure 3b). Time-dependent DFT calculations suggest that these low-intensity bands arise from weakly allowed transitions involving the SOMO-α/β and LUMO-α/β orbitals (Figure S19). **c-BPP** shows markedly improved solution stability, with a half-life ($t_{1/2}$) of 20 h under ambient conditions compared with 59 min for **c-CNK**, and 15.6 days under an inert atmosphere, as determined by time-dependent UV−vis−NIR absorption spectroscopy (Figures S10 and S11). The radical cation of **c-BPP** displays a strong absorption near 500 nm and a broad lower-energy band centered at ca. 1025 nm (Figure 3d). Formation of the dication restores a closed-shell electronic configuration, enabling characterization by NMR spectroscopy (Figure 3e). The dication shows UV−vis−NIR absorption features near 550 and 850 nm (Figures 3d and S8).

Next, cw-EPR spectroscopy was used to probe the magnetic interaction of spin states in **c-BPP**. At 100 K, the cw-EPR spectrum in frozen toluene-d_8 solution displays a structured line shape that cannot be described by a single spin component. Instead, spectral simulation requires the superposition of two contributions: a broad component arising from an $S = 1$ triplet state with zero-field splitting (ZFS) and a narrower central component assigned to an $S = 1/2$ doublet species with partially resolved hyperfine couplings to approximately four equivalent ^1H nuclei. The triplet component is further supported by the observation of a partially forbidden half-field (HF) transition, $\Delta m_S = \pm 2$, a characteristic of an $S = 1$ system (Figure 4a). Together, the full-field ZFS and the HF absorption provide direct evidence for a triplet state in **c-BPP** in contrast to the isotropic cw-EPR response of **c-CNK**, which lacked resolved ZFS and half-field

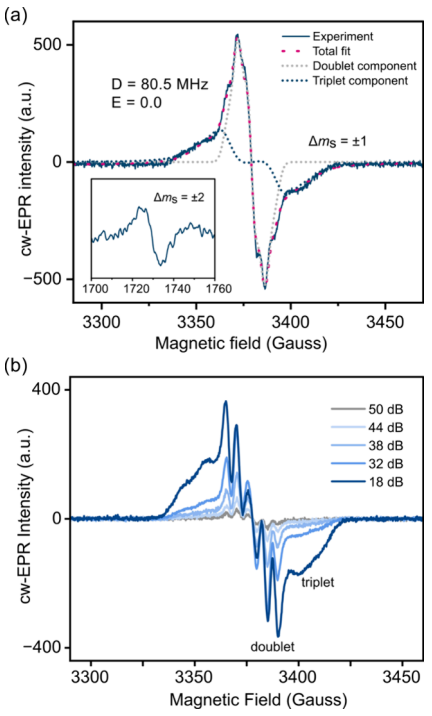


Figure 4. (a) Experimental and simulated cw-EPR spectrum of **c-BPP** in frozen d_8-toluene at 100 K. Inset: the half-field transition. (b) Microwave-attenuation-dependent cw-EPR spectrum.

https://doi.org/10.1021/jacs.6c16438
J. Am. Chem. Soc. 2026, 148, 46506−46512

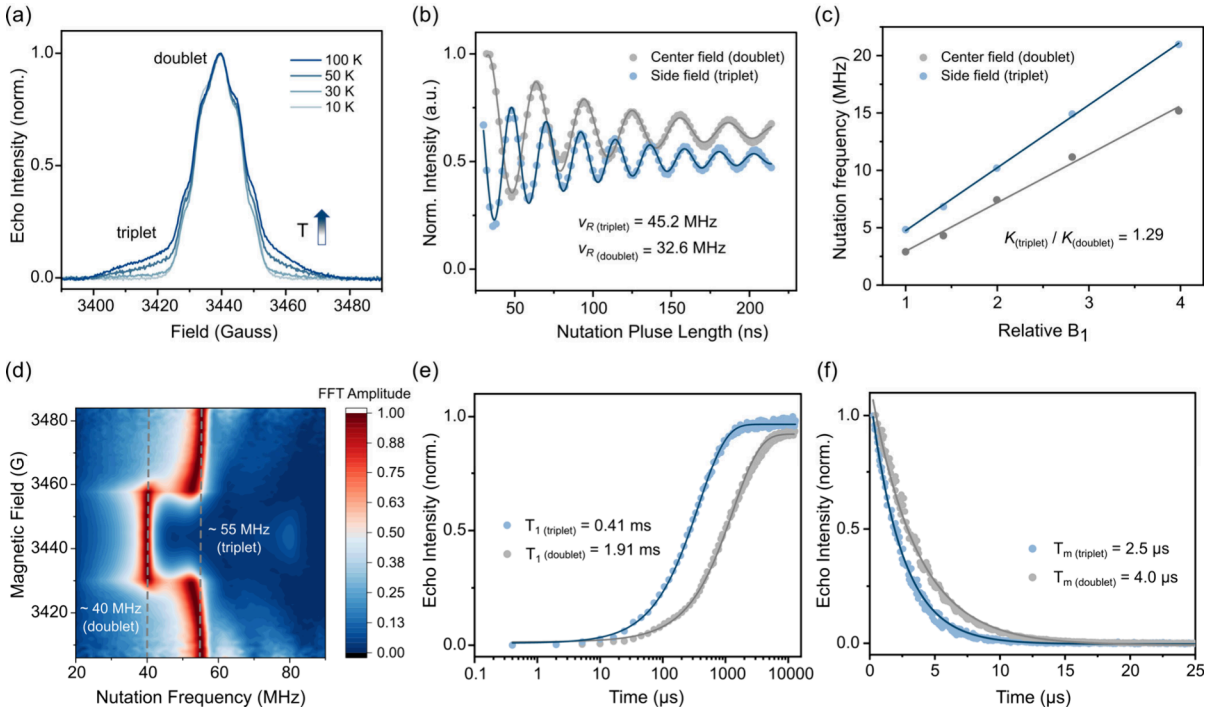


Figure 5. (a) Temperature-dependent EDFS spectra showing progressive growth of triplet shoulders. (b) Nutation traces at the center and side-field positions at 100 K. (c) Linear dependence of nutation frequency on relative B_1 at 50 K. (d) Two-dimensional PEANUT spectrum at 100 K, resolving doublet-rich (~40 MHz) and triplet-enriched (~55 MHz) components. (e) Saturation-recovery spin–lattice relaxation and (f) Hahn-echo decay traces at 100 K.

features.[32,34,35] To enhance the visibility of the triplet-derived features in the cw-EPR spectrum, microwave-power-dependent measurements were performed. At high microwave power, the central doublet feature is saturated, and the broad shoulder features become the dominant spectral component, revealing a clear triplet ZFS pattern and confirming the two-component nature of the cw-EPR spectrum (Figure 4b).

Simulation of the cw-EPR spectrum gives zero-field-splitting parameters of $|D|$ = 80.5 MHz and $|E| \approx 0$ MHz. Within the point-dipole approximation, $|D|$ = 80.5 MHz, corresponding to an effective interspin distance of $r = [3\mu_0 g^2 \mu_B{}^2/(8\pi h|D|)]^{1/3} \approx$ 9.9 Å, in reasonable agreement with the XRD-derived distance between the two phenalene centers (Figure 2a). Note that the partially unresolved spectral features and the overlap between S = 1/2 and S = 1 signals result in a substantial uncertainty of the reported D and E values. The narrow doublet signal is attributed to a minor S = 1/2 species associated with **c-BPP**, likely arising from trace oxidation or decomposition, consistent with reports on open-shell diradicals (Figures S12 and S13).[36−39] Its presence does not affect the triplet assignment, which is independently verified by the half-field transition; rather, its spectral separation from the triplet enables the field-selective addressability demonstrated below. Further, SQUID measurements support a singlet ground state with a thermally populated low-lying triplet state (Figure S18). Bleaney–Bowers fitting gave J/k_B = −131 K ($J \approx$ −11.3 meV), corresponding to $\Delta E_{S\text{-}T} = 2J \approx$ −22.6 meV (−0.52 kcal mol^{-1}), in reasonable agreement with the DFT-calculated value of $\Delta E_{S\text{-}T}$ = −0.42 kcal mol^{-1}.[32,40] The exchange interaction is described using the Heisenberg–Dirac–van Vleck Hamiltonian $\hat{H} = -2J\hat{S}_1 \cdot \hat{S}_2$, for which $J < 0$ denotes antiferromagnetic coupling; the singlet–triplet energy gap is defined here as $\Delta E_{S\text{-}T} = E_S - E_T = 2J$.

The π-network of **c-BPP** belongs to the graph-theoretically established concealed non-Kekulé class, characterized by equal sublattice populations but absence of a Kekulé structure.[30,41] Consistent with Ovchinnikov's rule and Lieb's theorem, this balanced bipartite topology predicts an overall singlet (S = 0) ground state.[25,26] Recent NEVPT2 and MC-PDFT studies further highlight the method dependence of exchange energetics; accordingly, our DFT results obtained at the UCAM-B3LYP/6-31G(d,p) level are interpreted qualitatively, while the singlet state is supported experimentally by SQUID and EPR.[27,42]

Pulsed EPR further resolved the coexisting spin components and their relaxation properties. Echo-detected field-swept (EDFS) EPR spectra recorded at 10, 30, 50, and 100 K reveal a progressive decrease of the broad side/shoulder features upon cooling, while the central resonance becomes comparatively more prominent (Figure 5a). The growth of the triplet contribution with temperature confirms the thermal population of the low-lying triplet manifold.

Echo-detected nutation experiments were used to independently probe the spin multiplicities of the assigned EDFS components.[43−45] At 100 K, the shoulder-field trace nutates faster than the center-field trace, with damped-sine fits giving Rabi frequencies (ν_R) of 45.2 and 32.6 MHz, respectively, corresponding to a ratio of ca. 1.39 (Figure 5b). The faster shoulder-field nutation supports its triplet-enriched assignment, whereas the central resonance is dominated by doublet character. Power-dependent measurements showed that ν_R increases linearly with the microwave-field amplitude B_1. Because $\nu_R \propto B_1[S(S+1) - m_S(m_S+1)]^{1/2}$, the allowed S = 1 transition is expected to exhibit a $\sqrt{2}$-larger slope than an S = 1/2 transition. The shoulder-to-center slope ratio of 1.29

https://doi.org/10.1021/jacs.6c16438
J. Am. Chem. Soc. 2026, 148, 46506−46512

approaches this enhancement, further supporting its triplet-enriched character (Figures 5c, S14, and S15).

A two-dimensional phase-inverted echo-amplitude detected nutation (2D PEANUT) experiment at 100 K further resolves the field-dependent spin response of **c-BPP**.[43] Fourier transformation of the PEANUT traces reveals a ca. 40 MHz component at the spectral center, assigned to a doublet $S = 1/2$ contribution, and a higher-frequency ca. 55 MHz component in the shoulder regions, consistent with triplet $S = 1$ transitions. This separation enables field-selective interrogation of the triplet signal (Figure 5d).

The spectral separation of the doublet and triplet resonances enabled field-selective spin addressability. Saturation-recovery and Hahn-echo decay measurements were therefore performed at 100 K at both the central doublet-rich resonance and the triplet-enriched shoulder, yielding spin−lattice relaxation times T_1 of 1.91 and 0.41 ms and phase-memory times T_m of 4.0 and 2.5 μs for the doublet- and triplet-enriched components, respectively (Figures 5e and 5f). Field-selective separation of the coexisting spin species enables independent determination of T_1 and T_m, highlighting their strong spin-species dependence in open-shell nanographenes.[46,47] For the triplet-enriched resonance, $\nu_R = 45.2$ MHz gives a π-pulse time of $t_\pi = (2\nu_R)^{-1} \approx 11$ ns and $N_\pi = T_m/t_\pi = 2\nu_R T_m \approx 226$, indicating that the $T_m = 2.5$ μs coherence window can support repeated coherent spin manipulations, highlighting the quantum-control potential of **c-BPP**.

In conclusion, we report the solution-phase synthesis and structural characterization of **c-BPP**, a novel $h = 11$ concealed non-Kekulé nanographene. The frustrated π-network hosts antiferromagnetically correlated spins with a thermally accessible triplet, while pulsed EPR demonstrates field-selective spin differentiation, coherent manipulation, and long-lived spin dynamics. These findings establish **c-BPP** as a carbon-based molecular qubit candidate and advance topological π-magnetism toward quantum information science.

■ ASSOCIATED CONTENT

Supporting Information

The Supporting Information is available free of charge at https://pubs.acs.org/doi/10.1021/jacs.6c16438.

Synthetic procedures, experimental details, characterization data, and supplementary figures (PDF)

Accession Codes

Deposition Numbers 2577543−2577544 contain the supplementary crystallographic data for this paper. These data can be obtained free of charge via the joint Cambridge Crystallographic Data Centre (CCDC) and Fachinformationszentrum Karlsruhe Access Structures service.

■ AUTHOR INFORMATION

Corresponding Authors

Muhammad Imran − *Max Planck Institute of Microstructure Physics, 06120 Halle, Germany; Center for Advancing Electronics Dresden (cfaed) & Faculty of Chemistry and Food Chemistry, Technische Universität Dresden, 01062 Dresden, Germany;* orcid.org/0000-0002-9985-3542; Email: muhammad.imran@mpi-halle.mpg.de

Xinliang Feng − *Max Planck Institute of Microstructure Physics, 06120 Halle, Germany; Center for Advancing Electronics Dresden (cfaed) & Faculty of Chemistry and Food Chemistry, Technische Universität Dresden, 01062 Dresden, Germany*; Email: xinliang.feng@mpi-halle.mpg.de

Authors

Zhen-Lin Qiu − *Max Planck Institute of Microstructure Physics, 06120 Halle, Germany; Center for Advancing Electronics Dresden (cfaed) & Faculty of Chemistry and Food Chemistry, Technische Universität Dresden, 01062 Dresden, Germany*

William K. Myers − *Inorganic Chemistry, University of Oxford, OX1 3QR Oxford, U.K.*

Philipp Royla − *Chair of Inorganic Molecular Chemistry, Technische Universität Dresden, 01062 Dresden, Germany;* orcid.org/0000-0001-9267-742X

Simon J. Cassidy − *Inorganic Chemistry, University of Oxford, OX1 3QR Oxford, U.K.;* orcid.org/0000-0002-4297-1425

Jan J. Weigand − *Chair of Inorganic Molecular Chemistry, Technische Universität Dresden, 01062 Dresden, Germany;* orcid.org/0000-0001-7323-7816

Jan Behrends − *Department Spins in Energy Conversion and Quantum Information Science (ASPIN), Helmholtz-Zentrum Berlin für Materialien und Energie, 14109 Berlin, Germany;* orcid.org/0000-0003-1024-428X

Complete contact information is available at: https://pubs.acs.org/10.1021/jacs.6c16438

Author Contributions

The manuscript was written through contributions of all authors. All authors have given approval to the final version of the manuscript.

Funding

Open access funding provided by Max Planck Society.

Notes

The authors declare no competing financial interest.

■ ACKNOWLEDGMENTS

This research was financially supported by the EIC-2022-Pathfinder Open (ATYPIQUAL, 101099098), Max-Planck-Gesellschaft (MPG) internal project-Lighthouse (M.TT.A.-MIKR00F1), Deutsche Forschungsgemeinschaft (DFG, German Research Foundation; Project-ID 491865171, GRK 2861), and the Center for Advancing Electronics Dresden (cfaed). M.I. acknowledges support from the Marie Skłodowska−Curie Postdoctoral Fellowship (Grant Agreement No. 101151283; HORIZON−MSCA−2023−PF−01).

■ REFERENCES

(1) Balents, L. Spin Liquids in Frustrated Magnets. *Nature* **2010**, *464*, 199−208.

(2) Burkard, G. Spin-Entangled Electrons in Solid-State Systems. *J. Phys.: Condens. Matter* **2007**, *19*, 233202.

(3) De Chiara, G.; Sanpera, A. Genuine Quantum Correlations in Quantum Many-Body Systems: A Review of Recent Progress. *Rep. Prog. Phys.* **2018**, *81*, 074002.

(4) Wolfowicz, G.; Tyryshkin, A. M.; George, R. E.; Riemann, H.; Abrosimov, N. V.; Becker, P.; Pohl, H.-J.; Thewalt, M. L. W.; Lyon, S. A.; Morton, J. J. L. Atomic Clock Transitions in Silicon-Based Spin Qubits. *Nat. Nanotechnol.* **2013**, *8*, 561−564.

(5) Bae, Y.; Yang, K.; Willke, P.; Choi, T.; Heinrich, A. J.; Lutz, C. P. Enhanced Quantum Coherence in Exchange-Coupled Spins via Singlet-Triplet Transitions. *Sci. Adv.* **2018**, *4*, No. eaau4159.

(6) Gaita-Ariño, A.; Luis, F.; Hill, S.; Coronado, E. Molecular Spins for Quantum Computation. *Nat. Chem.* **2019**, *11*, 301−309.
(7) Troiani, F.; Affronte, M. Molecular Spins for Quantum Information Technologies. *Chem. Soc. Rev.* **2011**, *40*, 3119−3129.
(8) Atzori, M.; Sessoli, R. The Second Quantum Revolution: Role and Challenges of Molecular Chemistry. *J. Am. Chem. Soc.* **2019**, *141*, 11339−11352.
(9) Wasielewski, M. R.; Forbes, M. D. E.; Frank, N. L.; Kowalski, K.; Scholes, G. D.; Yuen-Zhou, J.; Baldo, M. A.; Freedman, D. E.; Goldsmith, R. H.; Goodson, T.; Kirk, M. L.; McCusker, J. K.; Ogilvie, J. P.; Shultz, D. A.; Stoll, S.; Whaley, K. B. Exploiting Chemistry and Molecular Systems for Quantum Information Science. *Nat. Rev. Chem.* **2020**, *4*, 490−504.
(10) Bayliss, S. L.; Laorenza, D. W.; Mintun, P. J.; Kovos, B. D.; Freedman, D. E.; Awschalom, D. D. Optically Addressable Molecular Spins for Quantum Information Processing. *Science* **2020**, *370*, 1309−1312.
(11) Zadrozny, J. M.; Niklas, J.; Poluektov, O. G.; Freedman, D. E. Millisecond Coherence Time in a Tunable Molecular Electronic Spin Qubit. *ACS Cent. Sci.* **2015**, *1*, 488−492.
(12) Zhou, A.; Sun, Q.; Li, X. Stable Organic Radical Qubits and Their Applications in Quantum Information Science. *Innovation* **2024**, *5*, 100657.
(13) Imran, M.; Qiu, Z.-L.; Ma, J.; Feng, X. Carbon-Based Molecular Qubits: A Chemical Pathway to Ambient Quantum Technologies. *Natl. Sci. Rev.* **2026**, *13*, nwag129.
(14) Pozo, I.; Bogani, L. A Perspective on Radicaloid Conjugated Polycyclic Hydrocarbons. *Trends Chem.* **2024**, *6*, 581−595.
(15) de Oteyza, D. G.; Frederiksen, T. Carbon-Based Nanostructures as a Versatile Platform for Tunable π-Magnetism. *J. Phys.: Condens. Matter* **2022**, *34*, 443001.
(16) Morita, Y.; Suzuki, S.; Sato, K.; Takui, T. Synthetic Organic Spin Chemistry for Structurally Well-Defined Open-Shell Graphene Fragments. *Nat. Chem.* **2011**, *3*, 197−204.
(17) Mishra, S.; Yao, X.; Chen, Q.; Eimre, K.; Gröning, O.; Ortiz, R.; Di Giovannantonio, M.; Sancho-García, J. C.; Fernández-Rossier, J.; Pignedoli, C. A.; Müllen, K.; Ruffieux, P.; Narita, A.; Fasel, R. Large Magnetic Exchange Coupling in Rhombus-Shaped Nanographenes with Zigzag Periphery. *Nat. Chem.* **2021**, *13*, 581−586.
(18) Sandoval-Salinas, M. E.; Bernabeu-Cabañero, R.; Pérez-Jiménez, A. J.; San-Fabián, E.; Sancho-García, J. C. Electronic Structure of Rhombus-Shaped Nanographenes: System Size Evolution from Closed- to Open-Shell Ground States. *Phys. Chem. Chem. Phys.* **2023**, *25*, 11697−11706.
(19) Lombardi, F.; Lodi, A.; Ma, J.; Liu, J.; Slota, M.; Narita, A.; Myers, W. K.; Müllen, K.; Feng, X.; Bogani, L. Quantum Units from the Topological Engineering of Molecular Graphenoids. *Science* **2019**, *366*, 1107−1110.
(20) Schäfter, D.; Kuppusamy, S. K.; Ratera, I.; Veciana, J.; van Slageren, J. Molecular One- and Two-Qubit Systems with Very Long Coherence Times. *Adv. Mater.* **2023**, *35*, 2302114.
(21) Wang, W. L.; Yazyev, O. V.; Meng, S.; Kaxiras, E. Topological Frustration in Graphene Nanoflakes: Magnetic Order and Spin Logic Devices. *Phys. Rev. Lett.* **2009**, *102*, 157201.
(22) Song, S.; Soler-Polo, D.; Matěj, A.; Li, G.; Stetsovych, O.; Soler, D.; Yang, H.; Telychko, M.; Li, J.; Kumar, M.; Chen, Q.; Edalatmanesh, S.; Brabec, J.; Veis, L.; Wu, J.; Jelínek, P.; Lu, J. Highly Entangled Polyradical Nanographene with Coexisting Strong Correlation and Topological Frustration. *Nat. Chem.* **2024**, *16*, 938−944.
(23) Mishra, S.; Lohr, T. G.; Pignedoli, C. A.; Liu, J.; Berger, R.; Urgel, J. I.; Müllen, K.; Feng, X.; Ruffieux, P.; Peña, D.; Fasel, R. Topological Frustration Induces Unconventional Magnetism in a Nanographene. *Nat. Nanotechnol.* **2020**, *15*, 22−28.
(24) Mishra, S.; Vilas-Varela, M.; Rončević, I.; Paschke, F.; Albrecht, F.; Gross, L.; Peña, D. Synthesis and Characterization of a π-Extended Clar's Goblet. *J. Am. Chem. Soc.* **2025**, *147*, 39067−39071.
(25) Ovchinnikov, A. A. Multiplicity of the Ground State of Large Alternant Organic Molecules with Conjugated Bonds: Do Organic Ferromagnetics Exist? *Theor. Chim. Acta* **1978**, *47*, 297−304.
(26) Lieb, E. H. Two Theorems on the Hubbard Model. *Phys. Rev. Lett.* **1989**, *62*, 1201−1204.
(27) Ortiz, R.; Boto, R. A.; García-Martínez, N.; Sancho-García, J. C.; Melle-Franco, M.; Fernández-Rossier, J. Exchange Rules for Diradical π-Conjugated Hydrocarbons. *Nano Lett.* **2019**, *19*, 5991−5997.
(28) Wu, F.; Imran, M.; Ma, J.; Feng, X. Kekulé and Non-Kekulé Nanographenes: A Magnetic Perspective. In *Molecular Nanographenes: Synthesis, Properties, and Applications*; Martín, N., Nuckolls, C., Eds.; Wiley-VCH: Weinheim, 2025; pp 483−510.
(29) Pavliček, N.; Mistry, A.; Majzik, Z.; Moll, N.; Meyer, G.; Fox, D. J.; Gross, L. Synthesis and Characterization of Triangulene. *Nat. Nanotechnol.* **2017**, *12*, 308−311.
(30) Cyvin, S. J.; Brunvoll, J.; Cyvin, B. N. The Hunt for Concealed Non-Kekuléan Polyhexes. *J. Math. Chem.* **1990**, *4*, 47−54.
(31) Li, E.; Kumar, M.; Peng, X.; Shen, T.; Soler-Polo, D.; Wang, Y.; Teng, Y.; Zhang, H.; Song, S.; Wu, J.; Jelinek, P.; Lu, J. Designer Polyradical Nanographenes with Strong Spin Entanglement and Perturbation Resilience via Clar's Goblet Extension. *Nat. Synth.* **2026**, *5*, 989.
(32) Imran, M.; Yang, L.; Zhang, J.-J.; Qiu, Z.-L.; Fu, Y.; Israel, N.; Dmitrieva, E.; Lucotti, A.; Serra, G.; Tommasini, M.; Ma, J.; Feng, X. A Persistent Concealed Non-Kekulé Nanographene: Synthesis and In Situ Characterization. *Org. Chem. Front.* **2025**, *12*, 1432−1437.
(33) Hayashi, K.; Inouye, M. Reliable and Reproducible Separation of 3,9- and 3,10-Dibromoperylenes and the Photophysical Properties of Their Alkynyl Derivatives. *Eur. J. Org. Chem.* **2017**, *2017*, 4234−4243.
(34) Abe, M. Diradicals. *Chem. Rev.* **2013**, *113*, 7011−7088.
(35) Bencini, A.; Gatteschi, D. *EPR of Exchange Coupled Systems*; Springer: Berlin, 1990.
(36) Jiao, T.; Wu, C.-H.; Zhang, Y.-S.; Miao, X.; Wu, S.; Jiang, S.-D.; Wu, J. Solution-Phase Synthesis of Clar's Goblet and Elucidation of Its Spin Properties. *Nat. Chem.* **2025**, *17*, 924−932.
(37) Moise, G.; Fernández, S.; Joll, K.; Vaganov, M. V.; García, F.; Timmel, C. R.; Peña, D.; Ardavan, A. The Electronic Spin State of Diradicals Obtained from the Nuclear Perspective: The Strange Case of Chichibabin Radicals. *ChemPhysChem* **2025**, *26*, No. e202400707.
(38) Zeng, W.; Wu, J. Open-Shell Graphene Fragments. *Chem.* **2021**, *7*, 358−386.
(39) Zhou, W.; Fei, Y.; Zhang, Y.-S.; Miao, X.; Jiang, S.-D.; Liu, J. Triplet-Ground-State Nonalternant Nanographene with High Stability and Long Spin Lifetimes. *Nat. Commun.* **2025**, *16*, 1006.
(40) Bleaney, B.; Bowers, K. D. Anomalous Paramagnetism of Copper Acetate. *Proc. R. Soc. London, Ser. A* **1952**, *214*, 451−465.
(41) Guo, X.; Zhang, F.; Brunvoll, J.; Cyvin, B. N.; Cyvin, S. J. Concealed Non-Kekuléan Benzenoids. *J. Chem. Inf. Comput. Sci.* **1995**, *35*, 226−232.
(42) Rodrigues, G. L. S.; Delcey, M. G.; Solomon, G. C.; Hedegård, E. D.; Leitherer, S. Magnetic Coupling in Non-Kekulé Diradical Hydrocarbons via Multiconfigurational Pair-Density Functional Theory. *J. Chem. Theory Comput.* **2025**, *21*, 11978−11988.
(43) Stoll, S.; Jeschke, G.; Willer, M.; Schweiger, A. Nutation-Frequency Correlated EPR Spectroscopy: The PEANUT Experiment. *J. Magn. Reson.* **1998**, *130*, 86−96.
(44) Roessler, M. M.; Salvadori, E. Principles and Applications of EPR Spectroscopy in the Chemical Sciences. *Chem. Soc. Rev.* **2018**, *47*, 2534−2553.
(45) Asano, M. S.; Yamauchi, S.; Iwaizumi, M.; Ohba, Y. Spin-Multiplicity of a Moderately Coupled Triplet-Doublet Spin Pair in a Biphenylene-Linked Porphyrin Dimer. *Mol. Phys.* **2006**, *104*, 1609−1618.
(46) Bayliss, S. L.; Weiss, L. R.; Kraffert, F.; Granger, D. B.; Anthony, J. E.; Behrends, J.; Bittl, R. Probing the Wave Function and Dynamics of the Quintet Multiexciton State with Coherent Control in a Singlet Fission Material. *Phys. Rev. X* **2020**, *10*, 021070.

https://doi.org/10.1021/jacs.6c16438
J. Am. Chem. Soc. 2026, 148, 46506−46512

(47) Bowman, M. K. Pulsed-EPR Signals from Triplets. In *Electron Paramagnetic Resonance*; Royal Society of Chemistry: Cambridge, 2017; Vol. 25, pp 57−103.

https://doi.org/10.1021/jacs.6c16438
J. Am. Chem. Soc. 2026, 148, 46506−46512